Algorithmic quantum heat engines

Emre Köse,[1] Selçuk Çakmak,[2] Azmi Gençten,[3] Iannis K. Kominis,[4] and Özgür E. Müstecaplıoğlu[1,*]
[1]*Department of Physics, Koç University, 34450 Sariyer, İstanbul, Turkey*
[2]*Department of Software Engineering, Samsun University, 55420 Samsun, Turkey*
[3]*Department of Physics, Ondokuz Mayıs University, 55139 Samsun, Turkey*
[4]*Department of Physics, University of Crete, 70013 Heraklion, Greece*

(Received 23 January 2019; revised manuscript received 14 June 2019; published 8 July 2019)

We suggest alternative quantum Otto engines, using heat bath algorithmic cooling with a partner pairing algorithm instead of isochoric cooling and using quantum SWAP operations instead of quantum adiabatic processes. Liquid state nuclear magnetic resonance systems in a single entropy sink are treated as working fluids. The extractable work and thermal efficiency are analyzed in detail for four-stroke and two-stroke types of alternative quantum Otto engines. The role of the heat bath algorithmic cooling in these cycles is to use a single entropy sink instead of two so that a single incoherent energy resource can be harvested and processed using an algorithmic quantum heat engine. Our results indicate a path to programmable quantum heat engines as analogs of quantum computers beyond traditional heat engine cycles. We find that for our NMR system example implementation of quantum algorithmic heat engine stages yields more power due to increased cycle speeds.

DOI: 10.1103/PhysRevE.100.012109

I. INTRODUCTION

With the advances of miniaturized information and energy devices, the question of whether using a quantum system to harvest a classical resource can have an advantage over a classical harvester has gained much attention in recent years [1–24]. The argument is more or less settled in the case of quantum information devices, and the main challenge remaining concerns their efficient implementation. In typical quantum information devices, both the inputs and the algorithmic steps of operation are of completely quantum nature. In contrast, quantum energy devices process incoherent inputs and they operate with thermodynamical processes that are quantum analogs of their classical counterparts. The quantum superiority in such a thermal device reveals itself when the resource has some quantum character, for example, squeezing [25,26], or when the harvester has profound quantum nature, for example, quantum correlations [27,28]. Studies of both cases are limited to machine process analogs of classical thermodynamical ones. Here we ask how we can use genuine quantum steps in the machine operation and, if we can do so, what are the quantum advantages we can get.

For a specific system to explore completely quantum steps in thermal quantum device operation we examine an NMR system. Very recently NMR quantum heat engines have become experimentally available [29,30]. Power outputs of these machines are not optimized. One can use nonclassical resources, though such a resource would not be natural and may require some generation cost reducing overall operational efficiency. Alternatively one can use dynamical shortcuts to speed up adiabatic transformations [31] but this would increase experimental complexity, and moreover NMR thermalization is much slower, reducing the power output of the NMR machines.

Here, we propose to replace adiabatic steps by SWAP operations while replacing the cooling step by an algorithmic cooling [32–45]. By this way, NMR thermal device operation would closely resemble an NMR quantum computer [46–49] albeit processing a completely noisy input. We remark that there will be only the classical energy source as the input to the machine, while the second heat bath required by the second law of thermodynamics for work production would be an effective one, engineered by a spin ensemble, typical in the algorithmic cooling scheme. In addition to engine cycles, NMR systems were also proposed for studies of single-shot thermodynamics [50].

Our scheme allows us to provide at least one answer, in the context of NMR heat engines, to the question of how to implement genuine quantum steps in quantum machine operation to harvest a classical energy source. In addition, our calculations suggest that compared to the NMR engine with standard thermodynamical steps a quantum algorithmic NMR engine produces more power. The advantage comes from replacing the long-time isochoric cooling process with the more efficient and fast algorithmic cooling stage. We provide systematic investigation by first examining the case of the standard Otto cycle as a benchmark and then introducing the algorithmic cooling stage instead of the isochoric cooling one, and finally introducing the SWAP operation stages instead of the adiabatic transformations. Our results here can be seen as an example for a broader fundamental perspective that quantum computation processes can be used for efficient harvesting and processing of both the coherent information and the incoherent energy resources. From a practical point of view our approach suggests that quantum heat engines can be programed as analog quantum computers beyond traditional engine cycles.

*omustecap@ku.edu.tr

The organization of the paper is as follows. In Sec. II, we review the theory of the algorithmic heat engines based on heat bath algorithmic cooling (HBAC) in the cooling stage. In our heat engines, we take the parameters of a three-qubit NMR sample. The results and discussions are given in Sec. III. In Sec. III A, efficiency, work, and power output of the four-stroke algorithmic heat engines are discussed. By taking the same parameters to extract work we compare this engine with a standard quantum Otto engine cooled by isochoric stage. The two-stroke-type algorithmic engine results are given in Sec. III B. We conclude in Sec. IV. The details of the cooling algorithm and cost of cooling using HBAC with a partner pairing algorithm (PPA) are given in Appendix A.

II. THE WORKING FLUID

Quantum Otto engines (QOEs) consist of quantum adiabatic and isochoric processes [31]. Three types of the quantum heat engine are given in the literature as four-stroke, two-stroke, and continuous [1,14]. In this paper, we examine four-stroke and two-stroke types of QOEs. The basic model of HBAC with the PPA is advised instead of isochoric cooling. Implementation of HBAC requires two sets of qubits: reset qubits and computational qubits. One of the computational qubits operates as a target qubit which is going to be cooled by applying the PPA, while other computational qubits play a role in entropy compression [33]. This cooling process can be implemented with a minimal system composed of just three qubits [32–35].

The four-stroke algorithmic heat engine has two adiabatic stages, one isochoric stage, and one algorithmic cooling stage. For this engine, we only consider the target qubit as the working fluid (see Fig. 1). Reset and compression qubits are only used in the algorithmic cooling process, and their degrees of freedoms are traced out from the entire state of the system while determining the work output.

By "two-stroke engine," we refer to the original idea of the two-step work extraction given in Ref. [1], where it is called the "alternative Otto cycle." The idea is based upon earlier ones by Lloyd on NMR implementation of a quantum Maxwell demon [51]. It allows for genuine, all-quantum algorithmic steps to harvest work in contrast to the approach of mimicking classical engine cycles in quantum systems. The alternative Otto cycle is indeed a full quantum alternative to the Otto cycle; it replaces the cooling and adiabatic stages with HBAC and SWAP operations [or a series of controlled-NOT (CNOT) gate operations] and hence we compare it with the Otto cycles. Our approach is to come up with a quantum machine harvesting incoherent resources by cyclic quantum operations, the analog of quantum computers harvesting coherent (information) resources. For the working substance for two-stroke QOEs, we again choose the target qubit of the three-qubit system, but with an extra qubit coupled to the target qubit (see Fig. 2). In this engine, we have two qubits considered as working fluids.

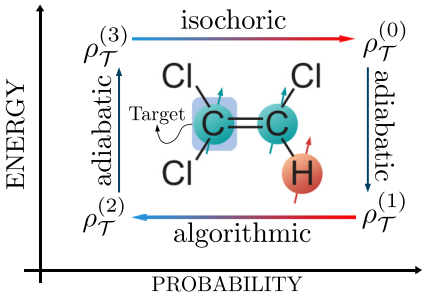

FIG. 1. Four-stroke algorithmic quantum heat engine operating in a single heat bath at temperature T. It has one isochoric heating process, two adiabatic processes, and one algorithmic cooling process.

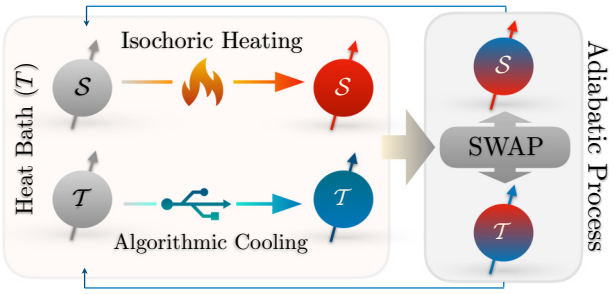

FIG. 2. Two-stroke algorithmic quantum heat engine operating in a single heat bath at temperature T. It has an isochoric heating process, the algorithmic cooling process happening at the same time, and then one adiabatic process using SWAP operation.

In NMR systems, various three-qubit models have been used for quantum information processing [52–55]. To make an applicable and realistic model for QOEs using these systems, a suitable sample and a well-designed procedure must be considered. We use parameters of $^{13}C_2$-trichloroethylene (TCE) (see Table I) with paramagnetic reagent $Cr(acac)_3$ in chloroform-d solution ($CDCl_3$) in our numerical calculations, which are also experimentally used for HBAC in Refs. [34,35]. Carbon-1 and carbon-2 qubits are classified as the target and the compression qubits. The hydrogen qubit is selected as the reset qubit because of the relaxation time, which is small compared to the other two qubits. To implement HBAC, the Hamiltonian of the three-qubit system in the laboratory frame can be written as [46]

$$H^{(0)} = -\hbar \sum_i \omega_i I_{iz} + \hbar \sum_{i \neq j} J_{ij} I_{iz} I_{jz}, \quad i, j = \{\mathcal{T}, \mathcal{C}, \mathcal{R}\}, \tag{1}$$

TABLE I. The first row in the table shows gyromagnetic ratio values of carbon 1, carbon 2, and hydrogen qubits. Regarding the 500-MHz NMR device, the corresponding characteristic frequencies are given in the second row. Also, their experimental τ_1 relaxation times are given in the third row. The last row shows J-coupling strength between these qubits [34,35].

	Target-C1	Compression-C2	Reset-H
$\gamma/2\pi$	10.7084 (MHz/T)	10.7084 (MHz/T)	42.477 (MHz/T)
$\omega/2\pi$	125.77 (MHz)	125.77 (MHz)	500.13 (MHz)
τ_1	43 (s)	20 (s)	3.5 (s)
	C1-C2	C1-H	C2-H
$J/2\pi$	103 (Hz)	9 (Hz)	200.8 (Hz)

where $\omega_i = \gamma_i B_z$ is the characteristic frequency of the ith qubit, γ_i is the nuclear gyromagnetic ratio, and B_z is the magnetic field. $\mathcal{T}$, $\mathcal{C}$, and $\mathcal{R}$ stand for target, compression, and reset qubits, respectively. I_z is the component of the spin angular momentum of the ith qubit and J_{ij} is the scalar isotropic coupling strength between ith and jth qubits.

III. RESULTS AND DISCUSSION

A. Four-stroke algorithmic heat engine

Typically, four-stroke QOEs consist of two isochoric and two adiabatic stages. Instead, we implement one algorithmic cooling stage instead of one of the isochoric stages (see Fig. 1). The adiabatic expansion stage leads to decrease of the level spacing of the qubits. This happens when the magnetic field decreases. In the opposite case, if the level spacing of the qubits is increasing then we call it "adiabatic compression." This allows for a more faithful representation of the classical Otto cycle terminology for our algorithmic engine. The details of the four-stroke cycle are described as follows.

1. Isochoric heating

The three-qubit TCE molecule with the Hamiltonian in Eq. (1) is in contact with a heat bath at temperature $T =$ 300 K. The density matrix of the three-qubit system at the end of this stage is given by the thermalized state as

$$\rho_{\rm th}^{(0)} = \frac{e^{-\beta H^{(0)}}}{Z}, \tag{2}$$

where $Z = \mathrm{Tr}[e^{-\beta H^{(0)}}]$ is the partition function and $\beta = 1/k_B T$. The initial density matrix of our working fluid (target qubit) can be expressed by taking a partial trace of the three-qubit system:

$$\rho_{\mathcal{T}}^{(0)} = \mathrm{Tr}_{\mathcal{C},\mathcal{R}}\big[\rho_{\rm th}^{(0)}\big]. \tag{3}$$

2. Adiabatic expansion

Qubits are isolated from the heat bath and undergo finite-time adiabatic expansion. The adiabatic processes of the cycle are assumed to be generated by a time-dependent magnetic field [56,57]. Here, $H^{(0)}$ at $t = 0$ is changed to $H^{(1)}$ at $t = \tau/2$ by driving the initial magnetic field as $B_z \to B_z/2$. The time evolution of the whole system is governed by the Liouville–von Neumann equation $\dot{\rho}(t) = -[H(t), \rho(t)]$. The initial state as a condition $(t = 0)$ is $\rho(0) = \rho_{\rm th}^{(0)}$, and $H(t)$ can be expressed as $H(t) = H^{(0)} + H_{\rm drive}$, where $H_{\rm drive}$ is given by $H_{\rm drive} = \hbar \sum_i (\omega_i - \omega_i')I_{iz} \sin(\pi t/\tau)$. At the end of the expansion, the Hamiltonian of the whole system is

$$H^{(1)} = -\hbar \sum_i \omega_i' I_{iz} + \hbar \sum_{i \neq j} J_{ij} I_{iz} I_{jz}. \tag{4}$$

Here, $\omega_i' = \omega_i/2$ is the characteristic frequency at the end of the adiabatic stage. Considering the state of the three-qubit system at the end of the expansion $(t = \tau/2)$ as $\rho^{(1)} = \rho(\tau/2)$, we can find the state of the target qubit as $\rho_{\mathcal{T}}^{(1)} = \mathrm{Tr}_{\mathcal{C},\mathcal{R}}[\rho^{(1)}]$. Up to this point, we have used the three-qubit Hamiltonians in Eqs. (1) and (4). However, to find the work performed in the stage, we only need to deal with the target qubit. Therefore, we can write the local Hamiltonian for the target qubit before the expansion as $H_{\mathcal{T}}^{(0)} = -\hbar\omega_{\mathcal{T}} I_z$ and at the end of the expansion as $H_{\mathcal{T}}^{(1)} = -\hbar\omega_{\mathcal{T}}' I_z$. Then, the work performed by the working fluid is

$$W_1 = \mathrm{Tr}\big[H_{\mathcal{T}}^{(0)} \rho_{\mathcal{T}}^{(0)}\big] - \mathrm{Tr}\big[H_{\mathcal{T}}^{(1)} \rho_{\mathcal{T}}^{(1)}\big]. \tag{5}$$

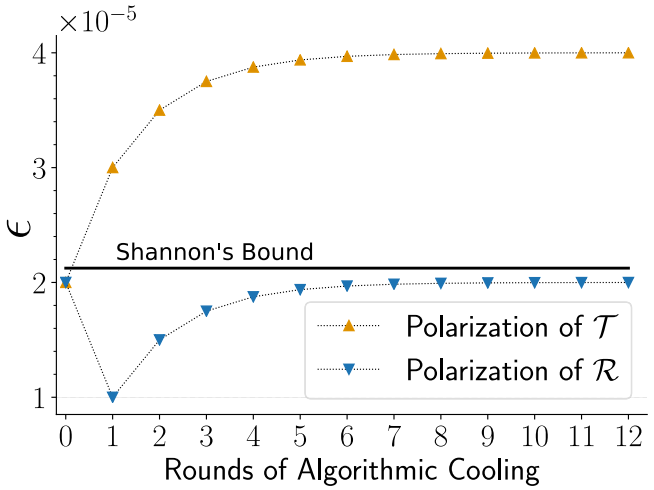

FIG. 3. The polarization ϵ (dimensionless) calculated by using Eq. (7) for each round of algorithmic cooling. The target and reset qubits polarizations are calculated by taking into account the perfectly applied quantum logic gates in terms of several rounds of the PPA. The black line shows Shannon's limit of polarization. The polarization of the target qubit has exceeded this limit after the first iteration, and the reset qubit stays under this limit.

3. Heat bath algorithmic cooling

In this part of the engine, we usually need a cold heat bath to cool down our target qubit. Instead of using a cold heat bath, the working fluid is treated in the same heat bath as isochoric heating at temperature $T = 300$ K. Reset and compression qubits play their role in this stage. They help us to implement HBAC to cool down the target qubit. In this stage the Hamiltonian of the whole system is given in Eq. (4), and the details of the cooling mechanism are given in Appendix A. For each qubit, polarization is defined as the difference in the probability of up and down states and easily found as

$$\epsilon_i = \tanh\left(\frac{\hbar\omega_i'}{2k_B T}\right). \tag{6}$$

In a closed quantum system, Shannon's bound limits the polarization of single spin in a collection of equilibrium spin systems. Using the PPA allows us to increase the polarization of the target qubit. Consequently, the target qubit is cooled down beyond Shannon's bound [34]. After the first SWAP before the PPA, polarizations of the target and reset qubits are equal to each other. The value of their polarization is given as the zeroth iteration in Fig. 3 as $\approx 2.0 \times 10^{-5}$. Then, several rounds of the PPA are applied. The target qubit reaches a polarization above the Shannon limit as a result of the first iteration of the PPA. The effective temperature of the target is determined by Eq. (7) and plotted in Fig. 4. Hence, the target qubit cools down to $\approx$50 K. After seven iterations, the polarization of the target almost reaches its maximum value as

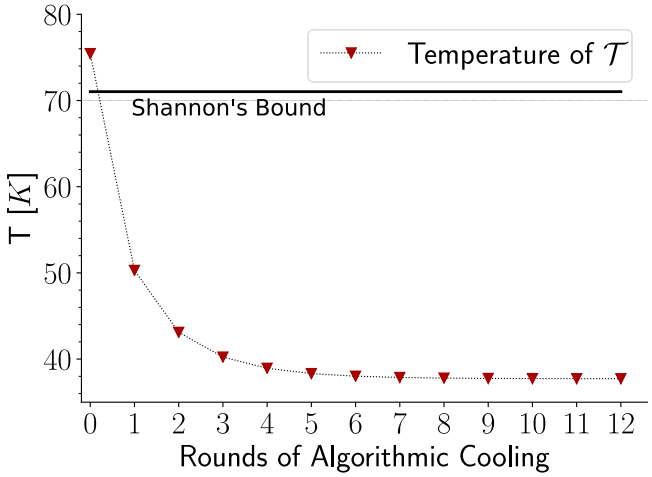

FIG. 4. The effective temperature of the target qubit calculated by using the relation between temperature and polarization given in Eq. (7). The black line shows the corresponding Shannon limit of temperature. The effective temperature of the target qubit has exceeded this limit after the first iteration.

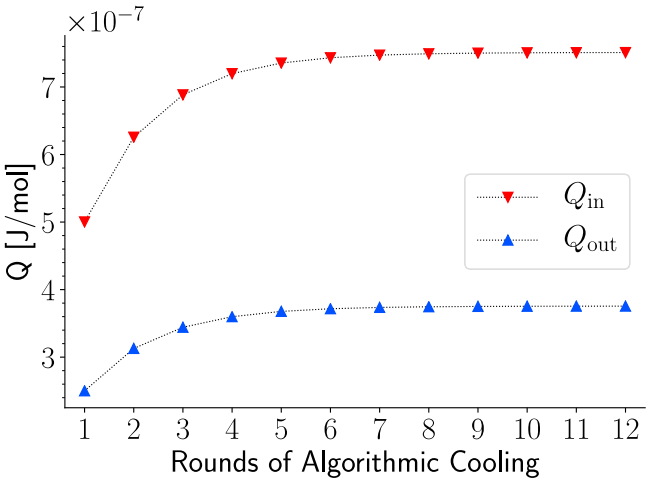

FIG. 5. Heat absorbed and released in a four-stroke cycle by the target qubit in the isochoric process (Q_{in}) and algorithmic cooling process (Q_{out}) per round of the PPA.

$\approx 4.0 \times 10^{-5}$ and the temperature of the target cools down to $\approx$37 K. At the end of the PPA, the density matrix of the target qubit is given by Eq. (A8) as

$$\rho_{\mathcal{T}}^{(2)} = \text{Tr}_{\mathcal{C},\mathcal{R}}[\rho^{(1,5)}], \tag{7}$$

where the first index of the three-qubit density matrix $\rho^{(1,5)}$ stands for the stage of the cycle and the second index from 0 to 5 indicates the state after each process of HBAC (see Appendix A).

The applied algorithm in this stage is done by external radio frequency (rf) field in the heat bath at temperature $T = 300$ K. We consider these rf pulses as a cost of cooling. In Appendix B, we calculate the required energy for the cooling process. We can safely say that our cost is above the work output of the four-stroke engine, which verifies the thermodynamical constraints.

4. Adiabatic compression

The Liouville–von Neumann equation gives the time evolution of the whole system during the adiabatic processes. In the compression step, $H^{(1)}$ at $t = 0$ is changed to $H^{(0)}$ at $t = \tau/2$ by driving back the magnetic field as $B_z/2 \rightarrow B_z$. The initial state ($t = 0$) of the total system is $\rho(0) = \rho^{(1,5)}$ before adiabatic compression. The state of the whole system after adiabatic compression ($t = \tau/2$) can be written as $\rho^{(3)} = \rho(\tau/2)$. Then, we can find the density matrix of the target qubit as $\rho_{\mathcal{T}}^{(3)} = \text{Tr}_{\mathcal{C},\mathcal{R}}[\rho^{(3)}]$. The work performed by the target qubit in this process can be written as

$$W_2 = \text{Tr}\big[H_{\mathcal{T}}^{(1)}\rho_{\mathcal{T}}^{(2)}\big] - \text{Tr}\big[H_{\mathcal{T}}^{(0)}\rho_{\mathcal{T}}^{(3)}\big]. \tag{8}$$

After this compression, the four-stroke algorithmic engine cycle is complete for the target qubit with state $\rho_{\mathcal{T}}^{(3)}$, and the states of the compression and reset qubits are $\rho_{\mathcal{C}}^{(3)} = \text{Tr}_{\mathcal{T},\mathcal{R}}[\rho^{(3)}]$ and $\rho_{\mathcal{R}}^{(3)} = \text{Tr}_{\mathcal{T},\mathcal{C}}[\rho^{(3)}]$, respectively. The next cycle again starts with the isochoric heating part and brings the whole system to the thermal state given in Eq. (2). This thermal state can be considered as the injection state when we first started the cycle. Then, the entire state of our system resets in every cycle with state $\rho^{(3)}$. Our choice of the order of the cycle steps is not unique and only for description purposes. As long as the cyclic order of the steps is respected, any of them can be designated as a last step.

5. Work and power output of the four-stroke QOE

The total work done by the working fluid at the end of the adiabatic stages can be found as $W = W_1 + W_2$. Alternatively, the same entire work can also be calculated, from the isochoric stage and algorithmic cooling stage, using the relation $W = Q_{\text{in}} - Q_{\text{out}}$ where $Q_{\text{in}} = \text{Tr}[H_{\mathcal{T}}^{(0)}(\rho_{\mathcal{T}}^{(0)} - \rho_{\mathcal{T}}^{(3)})]$ and $Q_{\text{out}} = \text{Tr}[H_{\mathcal{T}}^{(1)}(\rho_{\mathcal{T}}^{(1)} - \rho_{\mathcal{T}}^{(2)})]$ are the heat absorbed ($Q_{\text{in}} > 0$) and released ($-Q_{\text{out}} < 0$) in these stages. In Fig. 5, we plot the heat absorbed and released by the target qubit per round of the PPA. As the number of iterations increases, we observe that the absorbed heat increases more than the heat is released. After the first iteration, the target qubit absorbs $\approx 5 \times 10^{-7}$ J/mol of heat and releases $\approx 2.5 \times 10^{-7}$ J/mol of heat. As a result, $\approx 2.5 \times 10^{-7}$ J/mol work is performed. In Fig. 5, after seven iterations, the target qubit almost reaches the maximum value of the heat that it can absorb or release. Absorbed and released heat from the qubit in the cycle at this iteration is $\approx 3.5 \times 10^{-7}$ and $\approx 7.2 \times 10^{-7}$ J/mol. Thus, maximum work output of the cycle is $\approx 3.75 \times 10^{-7}$ J/mol.

To see the difference in power output caused by the algorithmic cooling and isochoric cooling, we numerically simulate a standard quantum Otto cycle cooled by isochoric cooling. Here, we imagine cold baths corresponding to the temperatures in Fig. 4, and we take the same parameters as we used for a four-stroke algorithmic heat engine. In the isochoric heating stage, we use a $\approx$300-K hot reservoir. In the adiabatic stages, we drive the frequency of the target qubit ($\omega_{\mathcal{T}} \rightleftarrows \omega'_{\mathcal{T}}$). The states of the target qubit at the end of isochoric cooling are equivalent to states at the end of algorithmic cooling. By this method, the work output of this standard QOE cooled by isochoric stage is the same as the cycle cooled by HBAC.

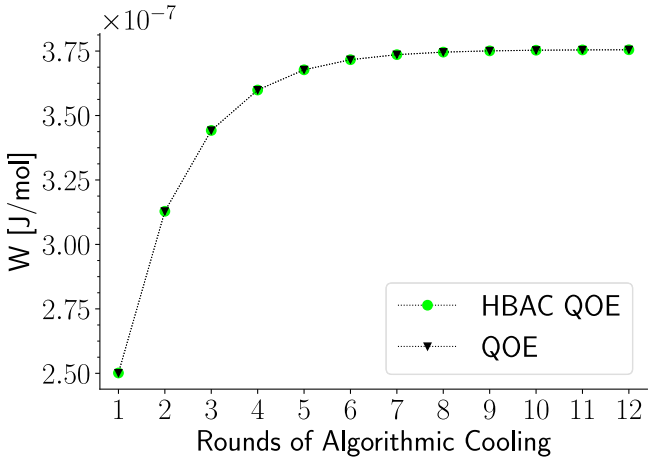

FIG. 6. Work obtained, in a four-stroke cycle per number of iterations of the PPA, from target qubits of 1 mol of TCE cooled by HBAC and work obtained from 1 mol of qubits, which are cooled by isochoric stage to temperatures corresponding to Fig. 4.

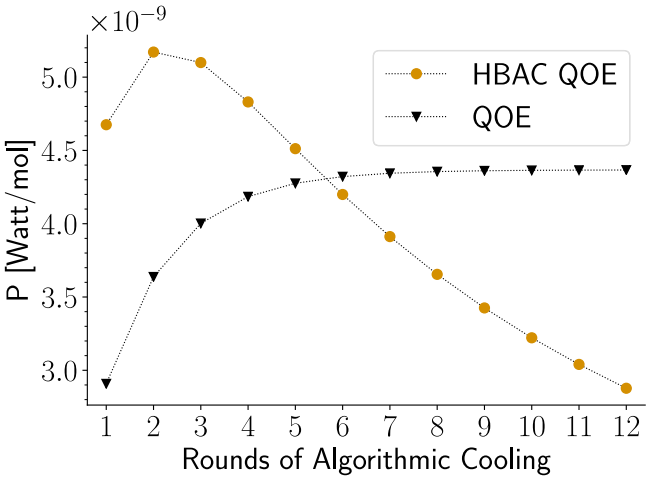

FIG. 7. Power output for a four-stroke cycle per number of iterations of the PPA, from target qubits of 1 mol TCE cooled by HBAC and from 1 mol of qubits cooled by isochoric stage to temperatures corresponding to Fig. 4.

In Fig. 6, for a four-stroke algorithmic heat engine, the work produced by the target qubit rapidly increases with the number of iterations; it remains constant after a specific iteration of the PPA. The reason for this behavior is that the HBAC can cool down the target qubit up to a certain limit [33,36,41,44], while for a standard QOE it increases due to the temperatures of the imagined cold baths. The amount of work corresponding to temperatures of $\approx$50 K is $\approx 2.5 \times 10^{-7}$ J/mol and for $\approx$37 K it is $\approx 3.75 \times 10^{-7}$ J/mol.

The adiabatic stages of the cycle are fast compared to the isochoric stages for a quantum Otto cycle using the NMR system as its working fluid [31]. Hence, we can estimate the power output of cycles, only taking isochoric steps and HBAC. In isochoric stages, we need to wait for the thermalization of the target qubit with the heat bath ($\tau_{\mathcal{T}}$). However, in the algorithmic cooling stage, the relaxation time of the reset qubit plays an important role. A single iteration of the PPA requires two reset process. Denoting the number of iterations by n, we can write the total time required to complete the algorithmic cooling stage as $\tau_{\mathcal{R}}(2n+1)$. Since both of the engines have the same work output, including the isochoric heating stage, the power output of the algorithmic heat engine becomes $P = W/[\tau_{\mathcal{T}} + \tau_{\mathcal{R}}(2n+1)]$, where $\tau_{\mathcal{T}}$ and $\tau_{\mathcal{R}}$ are relaxation times of the carbon-1 and hydrogen qubits from Table I, respectively. In the case of the standard quantum Otto cycle, the thermalization time in the cooling stage depends only on $\tau_{\mathcal{T}}$. Including the isochoric heating step, the power output becomes $P = W/2\tau_{\mathcal{T}}$. As long as $\tau_{\mathcal{R}}(2n+1) < \tau_{\mathcal{T}}$ is satisfied, which is the case up to the fifth iteration of the PPA with our parameters, then algorithmic heat engines will give more output compared to standard QOEs. In Fig. 7, we plot power outputs for both heat engines. We see that the second iteration of the PPA gives the maximum power output as $\approx 5.2 \times 10^{-9}$ W/mol for the algorithmic heat engine. As we can see, the number of iterations of the PPA is critical due to the optimum operation of the algorithmic quantum heat engine. More repetition means more R operation for the cycle so that the time required to complete the engine increases. As expected, the power output of the four-stroke algorithmic heat engine decreases as the number of iterations increases. After the fifth iteration of the PPA, the standard QOE using the isochoric cooling stage can dominate the engine using the algorithmic cooling stage. Accordingly, the optimum choice of the number of rounds for the PPA is 2 for our four-stroke model system. Such a choice optimizes the power output of the cycle, yielding high power performance.

It is vital to distinguish the cost paid to generate quantum gates from the cost to maintain the states of target qubit. The householding cost to maintain states in the working fluid can reduce thermodynamical efficiency [58,59]. In our case, we do not need to maintain target qubit states after the gates we have applied during the HBAC stage. The cost of generation of quantum gates is not included in thermodynamical efficiency of engines. Thus, we do not include the cost of algorithmic cooling in the efficiency of the engines. The efficiency of the cycle is determined by $\eta = 1 - \omega'_{\mathcal{T}}/\omega_{\mathcal{T}}$ and for this engine $\eta = 0.5$. Further, to see how the coupling terms affect the engine work output, we take the interaction terms as zero in the Hamiltonian and compare it with our results. Our numerical simulation shows the coupling between qubits brings a difference in the ninth order of magnitude to work output. Therefore we can ignore the effect of reset and compression qubits other than the algorithmic cooling step.

B. Two-stroke algorithmic heat engine

We also investigate the two-stroke QOE that is proposed in Refs. [1,14]. To construct it, we need to take two qubits donated as $\mathcal{S}$ and $\mathcal{T}$ as the working fluid. First, two qubits are isolated from each other. One of the qubits contacts with a heat bath at temperature T until it reaches equilibrium. Our purpose is to cool the other qubit within the same heat bath utilizing algorithmic cooling. Hence we need another two qubits for this process as compression qubit and reset qubit. This part is considered as two isochoric processes for the heat engine. Second, two qubits decouple from the heat

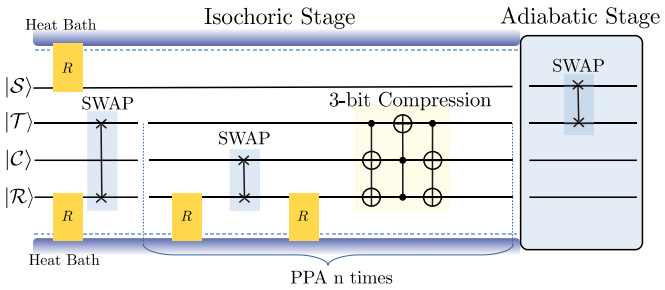

FIG. 8. Quantum circuit demonstrating the two-stroke heat bath algorithmic cooled quantum Otto engine. $|\mathcal{S}\rangle$ stands for qubit $\mathcal{S}$ and $|\mathcal{T}\rangle$ stands for qubit $\mathcal{T}$. Here, isochoric heating is demonstrated as an R operation and applied only one time on qubit $\mathcal{S}$. For qubit $\mathcal{T}$, the PPA is applied, and it is given in Appendix A. Then, these two processes complete the SWAP operation applied between two qubits and the cycle is completed with the adiabatic process.

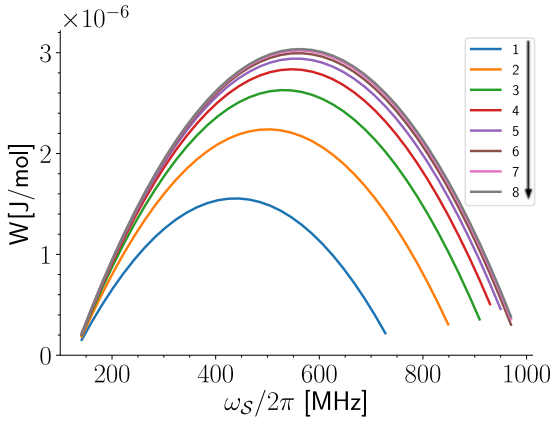

FIG. 9. Positive work obtained in two-stroke HBAC-QOE as a function of $\omega_{\mathcal{S}}$. The legend of the plot shows the number of rounds of the PPA applied to qubit $\mathcal{T}$ and the direction of the arrow indicates an increase in work output from first iteration to eighth iteration.

bath. Then, the SWAP operation is performed between these two qubits (see Fig. 8). The local Hamiltonian of the qubit $\mathcal{S}$ and qubit $\mathcal{T}$ can be written as $H_{\mathcal{S}} = -\hbar\omega_{\mathcal{S}} I_z$ and $H_{\mathcal{T}} = -\hbar\omega_{\mathcal{T}} I_z$, respectively. The density matrix of qubit $\mathcal{S}$ at the end of the isochoric stage is a thermalized state given by $\rho_{\mathcal{S}}^{(1)} = e^{-\beta H_{\mathcal{S}}}/Z$. For the algorithmic cooling, again we take a system with the Hamiltonian given in Eq. (1). Initially, assume that this three-qubit system is in a thermal equilibrium state $(\rho^{(1)})$ with the heat at temperature $T = 300$ K. Then we can cool down the qubit $\mathcal{T}$, using the algorithmic cooling given in Appendix A. The density matrix of qubit $\mathcal{T}$ at the end of HBAC can be written as $\rho_{\mathcal{T}}^{(1)} = \mathrm{Tr}_{\mathcal{C},\mathcal{R}}[\rho^{(1,5)}]$. It is assumed that the coupling between $\mathcal{S}$ and $\mathcal{T}$ qubits is small compared to $\omega_{\mathcal{S}}$ and $\omega_{\mathcal{T}}$. Thus, the density matrix of the total working fluid can be expressed as

$$\rho_{\mathcal{S},\mathcal{T}}^{(1)} \approx \rho_{\mathcal{S}}^{(1)} \otimes \rho_{\mathcal{T}}^{(1)}. \tag{9}$$

In the adiabatic process, a SWAP gate is applied to exchange the states of $\mathcal{S}$ and $\mathcal{T}$ qubits:

$$\rho_{\mathcal{S},\mathcal{T}}^{(2)} = \mathrm{SWAP}\big(\rho_{\mathcal{S},\mathcal{T}}^{(1)}\big)\mathrm{SWAP}^{\dagger}. \tag{10}$$

At the end of the cycle, density matrices of individual qubits become

$$\rho_{\mathcal{S}}^{(2)} = \mathrm{Tr}_{\mathcal{T}}\big[\rho_{\mathcal{S},\mathcal{T}}^{(2)}\big], \quad \rho_{\mathcal{T}}^{(2)} = \mathrm{Tr}_{\mathcal{S}}\big[\rho_{\mathcal{S},\mathcal{T}}^{(2)}\big]. \tag{11}$$

Heat absorbed by the qubit $\mathcal{S}$ is calculated as follows:

$$Q_{\mathrm{in}} = \mathrm{Tr}\big[H_{\mathcal{S}}\big(\rho_{\mathcal{S}}^{(1)} - \rho_{\mathcal{S}}^{(2)}\big)\big], \tag{12}$$

and the heat released by the qubit $\mathcal{T}$ is

$$Q_{\mathrm{out}} = \mathrm{Tr}\big[H_{\mathcal{T}}\big(\rho_{\mathcal{T}}^{(2)} - \rho_{\mathcal{T}}^{(1)}\big)\big]. \tag{13}$$

The net work is evaluated by $W = Q_{\mathrm{in}} - Q_{\mathrm{out}}$, with efficiency $\eta = 1 - \omega_{\mathcal{T}}/\omega_{\mathcal{S}}$. To get a positive work, the frequency of the qubit $\mathcal{S}$ needs to be higher than the frequency of the qubit $\mathcal{T}$ $(\omega_{\mathcal{S}} > \omega_{\mathcal{T}})$. In addition, $T > T_{\mathcal{T}}(\omega_{\mathcal{S}}/\omega_{\mathcal{T}})$ needs to be satisfied. Here $T_{\mathcal{T}}$ is the temperature of the target qubit in HBAC. Positive work conditions then can be expressed as

$$\omega_{\mathcal{T}} < \omega_{\mathcal{S}} < \omega_{\mathcal{T}} \frac{T}{T_{\mathcal{T}}}. \tag{14}$$

The work output of the two-stroke algorithmic quantum heat engine depends on the $\omega_{\mathcal{S}}$ and the number of iterations applied in the algorithmic cooling process. Figure 9 shows the relation between the work output and $\omega_{\mathcal{S}}$, for different numbers of iterations. When the number of iterations of the PPA increases, the best work output also increases. However, after some iteration, it remains almost constant due to limiting of the PPA to cool the qubit $\mathcal{T}$. It is found that for 580 MHz we almost get the best work output at the fifth iteration as $\approx 3.0 \times 10^{-6}$ J/mol. But this frequency does not give us the best work output at the first iteration. With 430-MHz frequency, we get $\approx 1.5 \times 10^{-6}$ J/mol maximum work output in the first iteration.

The adiabatic stage is evaluated by a SWAP operation, which is fast compared to the HBAC. Relaxation time of the $\mathcal{S}$ qubit may be estimated by considering spectral density functions $J(\omega, t_c)$, where t_c is the correlation time [48,60]. If we look for the optimum power output, the $\omega_{\mathcal{S}}$ is close to the frequency of the $\mathcal{R}$ qubit. If the environmental effects are the same, t_c may be assumed to be the same for the $\mathcal{R}$ and $\mathcal{S}$ qubit. As a result, we can say that the $\mathcal{S}$ qubit is thermalized until the HBAC process is complete. Thus, estimation of the power output for a two-stroke algorithmic heat engine depends only on the algorithmic cooling stage. Then, we can write the power output as $P = W/\tau_{\mathcal{R}}(2n+1)$ considering the relaxation time of the reset qubit and the number of iterations of the PPA. The relaxation time of hydrogen $(\tau_{\mathcal{R}})$ is given in Table I. In Fig. 10, we plot the power output based on the frequency of the $\mathcal{S}$ qubit for different iteration numbers. As expected, the power of the two-stoke algorithmic machine decreases as the number of iterations increases in contrast to the work. The optimum value is given as $\approx 1.47 \times 10^{-7}$ W/mol during the first iteration with 430-MHz frequency of the $\mathcal{S}$ qubit. If we compare these results to four-stroke quantum Otto cycles both cooled by HBAC and isochoric cooling, we see that the two-stroke cycle gives more work and power output. The efficiency of the cycle as a function of $\omega_{\mathcal{S}}$ is given above. Taking the optimum value for the power output during the first iteration with 430-MHz frequency of qubit $\mathcal{S}$, we find the efficiency of the two-stroke machine as 0.7. Based on these results, we can say that the two-stroke algorithmic heat engine is more efficient than four-stroke cycles.

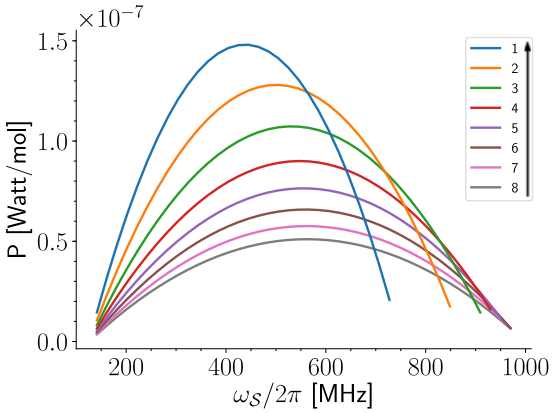

FIG. 10. Power output obtained in a two-stroke quantum Otto cycle for the different numbers of iterations of the PPA as a function of $\omega_{\mathcal{S}}$. The legend of the plot shows the number of rounds of the PPA applied to qubit $\mathcal{T}$ and the direction of the arrow indicates an increase in the power output from eighth iteration to first iteration.

To compare the algorithmic and the standard two-stroke heat engines, we again consider a two-stroke machine cooled with isochoric cooling. For isochoric cooling, we imagine cold heat baths for temperatures corresponding to the algorithmic cooling results for each iteration. When isochoric heating and adiabatic parts are applied in the same way, the work outputs that we get will be the same in these two machines. Assuming that the qubit $\mathcal{S}$ is thermalized faster than the qubit $\mathcal{T}$ during isochoric cooling, the power output of this standard two-stroke heat engine can only be determined by the thermalization time of the qubit $\mathcal{T}$ as $P = W/\tau_{\mathcal{T}}$. We can say that if $\tau_{\mathcal{R}}(2n+1) < \tau_{\mathcal{T}}$ is satisfied, which is the case up to the fifth iteration of the PPA with these parameters, our two-stroke algorithmic quantum heat engine gives more power output. Also, the second, lower temperature, bath is challenging to implement in the context of NMR systems, and that is why our main objective is to be able to harvest work out of the single common environment using HBAC.

IV. CONCLUSIONS

We have investigated the possible quantum Otto engines implementing HBAC instead of isochoric cooling. Conventional NMR setups do not allow one to change the strength (which is very large) of the magnetic field along the z direction. To solve this restriction, a NMR setup can be modified to change the strong magnetic field via gradient coils such as a magnetic resonance imaging system. Additionally, the sample is always in a single entropy sink in NMR systems. This is a critical challenge in designing QOEs, which requires two heat baths to extract work from NMR qubits. Using HBAC allows us to cool the working fluid in a single heat bath. Here we specifically showed that this cooling process could be implemented to four-stroke and two-stroke QOEs. The isochoric cooling process of the cycle takes too much time compared to the HBAC. Comparing our results with a single spin NMR heat engine, utilizing the HBAC for QOEs improves the power output of the cycles up to a particular iteration of the PPA. By using SWAP operations in place of adiabatic stages and HBAC instead of isochoric cooling, a completely algorithmic quantum heat engine, which can be more powerful and fast relative to those based upon traditional heat engine cycles, is proposed. Such engines offer programmable quantum heat engines as analogs of quantum computers but for efficient harvesting and processing of incoherent resources rather than coherent information resources.

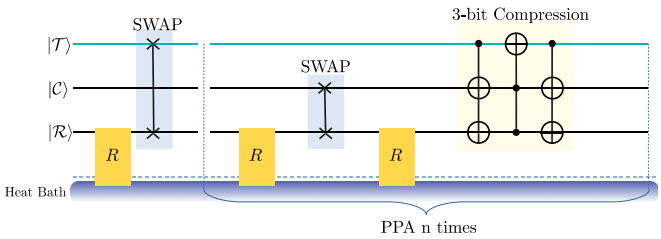

FIG. 11. Quantum circuit demonstrating the partner pairing algorithm for the three-qubit system given in Ref. [33]. $|\mathcal{T}\rangle$, $|\mathcal{C}\rangle$, and $|\mathcal{R}\rangle$ stand for target, compression, and reset qubits, respectively. The R process indicates the relaxation of the reset qubit. In the PPA, the first reset process is applied only one time. Then, the iteration part consists of SWAP and three-bit compression operations applied n times.

ACKNOWLEDGMENT

The authors thank M. Paternostro for fruitful discussions.

APPENDIX A: HEAT BATH ALGORITHMIC COOLING: THE PARTNER PAIRING ALGORITHM

We implement HBAC with the PPA (see Fig. 11), which uses quantum information processing to increase the purification level of qubits in NMR systems [32,33]. Before starting the PPA, the individual density matrices of the target, the compression, and the reset qubits are $\rho_{\mathcal{T}}^{(1)} = \mathrm{Tr}_{\mathcal{C},\mathcal{R}}[\rho^{(1)}]$, $\rho_{\mathcal{C}}^{(1)} = \mathrm{Tr}_{\mathcal{T},\mathcal{R}}[\rho^{(1)}]$, and $\rho_{\mathcal{R}}^{(1)} = \mathrm{Tr}_{\mathcal{T},\mathcal{C}}(\rho^{(1)})$, respectively, and $\rho^{(1)}$ is the initial density matrix of the three-qubit system. The reset has a small relaxation time compared to the target ($\tau_R \ll \tau_T$) and the compression ($\tau_R \ll \tau_C$) qubit, where $\tau_{\mathcal{T}}$, $\tau_{\mathcal{C}}$, and $\tau_{\mathcal{R}}$ are given in Table I, respectively. In each step of HBAC, R operation is applied to the reset qubit to thermalize it with the heat bath ($\rho_{\mathcal{R}}^{(1)} \to \rho_{\mathcal{R},\mathrm{th}}^{(1)}$) at temperature T. Scalar couplings between qubits are small compared to ω_i values. If we write the total density matrix of three qubits as a tensor product of the individual states, the fidelity of the density matrix in Eq. (2) and this product density matrix numerically is found to be close to 1. Thus, at the first step, the density matrix of the three-qubit system can be written as a tensor product of these states:

$$\rho^{(1,0)} = \rho_{\mathcal{T}}^{(1)} \otimes \rho_{\mathcal{C}}^{(1)} \otimes \rho_{\mathcal{R},\mathrm{th}}^{(1)}, \tag{A1}$$

where the first index of $\rho^{(1,0)}$ stands for the stage of the cycle, and the second index from 0 to 5 indicates the state after each process of HBAC. After the reset qubit regains its polarization, a unitary SWAP operator is used to exchange polarizations of the target and the reset qubit:

$$\rho^{(1,1)} = \mathrm{SWAP}_{\mathcal{T},\mathcal{R}}(\rho^{(1,0)})\,\mathrm{SWAP}_{\mathcal{T},\mathcal{R}}^{\dagger}. \tag{A2}$$

The states of the target and compression qubits become $\rho_{\mathcal{T}}^{(1,1)} = \mathrm{Tr}_{\mathcal{C},\mathcal{R}}[\rho^{(1,1)}]$ and $\rho_{\mathcal{C}}^{(1,1)} = \mathrm{Tr}_{\mathcal{T},\mathcal{R}}[\rho^{(1,1)}]$, respectively. After the unitary evolution, the PPA can be applied n times, which is given as follows.

(1) The reset qubit is thermalized with the heat bath. The density matrix of the three-qubit system becomes

$$\rho^{(1,2)} = \rho_{\mathcal{T}}^{(1,1)} \otimes \rho_{\mathcal{C}}^{(1,1)} \otimes \rho_{\mathcal{R},\mathrm{th}}^{(1)}. \tag{A3}$$

(2) SWAP is applied to change polarization between the compression and the reset qubit, such that

$$\rho^{(1,3)} = \mathrm{SWAP}_{\mathcal{C},\mathcal{R}}(\rho^{(1,2)})\,\mathrm{SWAP}_{\mathcal{C},\mathcal{R}}^{\dagger}. \tag{A4}$$

Then, the states of the target and the compression qubits become $\rho_{\mathcal{T}}^{(1,3)} = \mathrm{Tr}_{\mathcal{C},\mathcal{R}}[\rho^{(1,3)}]$ and $\rho_{\mathcal{C}}^{(1,3)} = \mathrm{Tr}_{\mathcal{T},\mathcal{R}}[\rho^{(1,3)}]$.

(3) The reset qubit regains its polarization. The state of the three-qubit system is expressed as

$$\rho^{(1,4)} = \rho_{\mathcal{T}}^{(1,3)} \otimes \rho_{\mathcal{C}}^{(1,3)} \otimes \rho_{\mathcal{R},\mathrm{th}}^{(1)}. \tag{A5}$$

(4) To lower the entropy of the target qubit and to increase the entropy of the reset qubit a 3-bit compression gate is applied to the density matrix:

$$\rho^{(1,5)} = \mathrm{COMP}(\rho^{(1,4)})\,\mathrm{COMP}^{\dagger}, \tag{A6}$$

where COMP is the unitary operation of the compression gate composed of unitary operators as two CNOT-NOT gates and a TOFFOLI gate, which can be expressed as

$$\mathrm{COMP} = [\mathrm{CNOT\text{-}NOT}][\mathrm{TOFFOLI}][\mathrm{CNOT\text{-}NOT}]. \tag{A7}$$

At the end of this iterative step the target qubit is cooled and the density matrix of it becomes

$$\rho_{\mathcal{T}}^{(2)} = \mathrm{Tr}_{\mathcal{C},\mathcal{R}}[\rho^{(1,5)}]. \tag{A8}$$

APPENDIX B: COST OF HEAT BATH ALGORITHMIC COOLING

The cost of cooling the target qubit using the HBAC in the engine is examined by coherent operations (rf applied externally to the system). The cost of coherent operations is treated as the free energy change of the system [61–63] or it can be estimated from absorption power of the rf field applied to generate quantum gates.

1. Coherent operations

From Appendix A, we know the states before and after the SWAP and COMP operations. Since the entropy of the whole system is invariant under a unitary operation, the free energy change for the first SWAP will be

$$\Delta F = \mathrm{Tr}[H^{(1)}(\rho^{(1,1)} - \rho^{(1,0)})]. \tag{B1}$$

In the iterative part of the PPA, for the first SWAP it will be

$$\Delta F' = \mathrm{Tr}[H^{(1)}(\rho^{(1,3)} - \rho^{(1,2)})], \tag{B2}$$

and for COMP operation

$$\Delta F'' = \mathrm{Tr}[H^{(1)}(\rho^{(1,5)} - \rho^{(1,4)})]. \tag{B3}$$

The total free energy change due to unitary operations will be

$$\Delta F_{\mathrm{tot}} = \Delta F + \Delta F' + \Delta F''. \tag{B4}$$

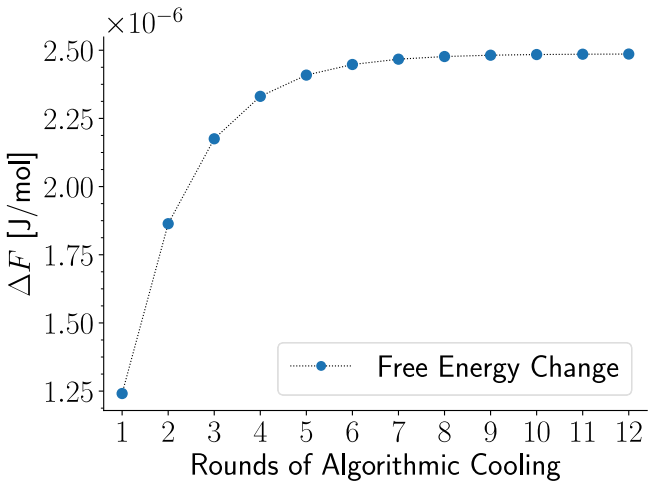

FIG. 12. The total cost of cooling the target qubit by HBAC. It is obtained by the free energy change due to unitary operations.

In Fig. 12, we plot total free energy change due to rounds of algorithmic cooling. From the plot we can see that our cost for unitary operations is above the work we gained from four-stroke algorithmic heat engines, and for a single iteration our cost is around $\Delta F \approx 1.2 \times 10^{-6}$ J/mol. After each unitary evolution in HBAC, the reset qubit is in nonequilibrium with the heat bath. So, R operation is done by the bath, and heat is released from the reset qubit to the thermal environment.

2. Rf field absorption energy

For a single pulse, we can calculate absorption energy, by a single qubit, using the nonrelativistic Fermi "golden rule" [48]. The unperturbed local Hamiltonian of the single qubit after adiabatic compression is $H_i^{(1)} = -\hbar\omega_i' I_z$, and the rf Hamiltonian as a perturbation can be written as

$$H_{\mathrm{rf}} = \tfrac{1}{2}\gamma_i \hbar B_{\mathrm{rf}}(I_+ e^{-i\omega t} + I_- e^{i\omega t}). \tag{B5}$$

For the spin 1/2 system the transition probability can be found as

$$W_{-\frac{1}{2}\to\frac{1}{2}} = \frac{\pi}{2}\gamma^2 B_{\mathrm{rf}}^2 f(\omega), \tag{B6}$$

where $f(\omega)$ is related to the shape of the pulse $\int f(\omega)d\omega = 1$. For instance, for the Lorentz shape it is described as $f(\omega) = \tau_2/\pi[1 + (\omega - \omega_i')^2\tau_2^2]$. Here, τ_2 is the transverse relaxation time. Usually, $\omega = \omega_i'$ and $f(\omega) = \tau_2/\pi$. If the difference in populations in a heat bath at temperature T can be written as $\approx \hbar\omega_i'/(2k_BT)$, then the amount of rf field energy absorbed per unit time by a single qubit can be found as

$$\begin{aligned}\mathcal{P} &= \hbar\omega_i'\left(\frac{\hbar\omega_i'}{2k_BT}\right)W_{-\frac{1}{2}\to\frac{1}{2}} \\ &= \frac{\pi\hbar^2\omega_i'^2}{4k_BT}\left(\gamma_i^2 B_{\mathrm{rf}}^2\right)f(\omega).\end{aligned}$$

Now we can determine pulse duration as $\theta_p = \gamma_i B_{\mathrm{rf}} t_p$ and for the $\pi/2$ pulse it can be found as $t_p = \pi/(2\gamma_i B_{\mathrm{rf}})$. So total absorbed energy for the single qubit will be

$$E_{\mathrm{abs}} = \mathcal{P}t_p = \frac{\pi\hbar^2\omega_i'^2}{8k_BT}(\gamma_i B_{\mathrm{rf}})\tau_2. \tag{B7}$$

The radio frequency field is applied to only one qubit during a CNOT gate and the NMR pulse sequence of the CNOT is given as $R_x(\pi/2)U(1/2J)R_y(\pi/2)$, where $R_i(\theta_p)$ is the rotation matrix applied in the ith direction and U is the unitary evolution due to the coupling of two qubits [46]. According to the first qubit orientation, the second qubit is reversed or not reversed. For a single CNOT, we need to apply two pulses in the x and y direction. SWAP operation also can be decomposed into three CNOT gates. So, for a single SWAP, one needs six pulses, and for the COMP gate we can assume it is around 10. In total, we approximately need 25 pulses for a single iteration of algorithmic cooling. At this stage, the frequency of the target and compression qubit is $\omega'_{\mathcal{T},\mathcal{C}} \approx 63$ MHz, and for the reset qubit $\omega'_{\mathcal{R}} \approx 250$ MHz. The temperature of the bath is 300 K. To estimate a rough result for a typical liquid state NMR system taking $\omega'_i \sim 100$ MHz, and assuming $\gamma_i B_{\rm rf} \sim 10^3$ Hz and $\tau_2 \sim 10$ ms, we can find the total energy absorbed by a single TCE molecule during the cooling process as $E_{\rm tot} \sim 2.6 \times 10^{-30}$ J. For 1 mol of TCE, it can be easily estimated as $E_{\rm tot} \sim 1.6 \times 10^{-6}$ J/mol. This result is pretty close to the above found by Eq. (B4) for a single iteration.

3. Rf field energy

We can also estimate the total energy given by every pulse due to the magnetic field. Since there will be losses to the environment, the rf field energy that we applied will be higher than the free energy change or absorption energy by spins. The energy density of the applied magnetic field can be written as

$$u = \frac{1}{2\mu_0}|B_{\rm rf}|^2. \tag{B8}$$

Local pulse intensity is found by simply multiplying this expression with c (speed of the field in vacuum):

$$I_p = cu = \frac{c}{2\mu_0}|B_{\rm rf}|^2. \tag{B9}$$

For a beam with a width of δ, the pulse energy can be written

$$U_p = I_p \pi(\delta/2)^2 t_p. \tag{B10}$$

Here, width δ is directly related to rf coil diameter assuming it is $\delta \sim 1$ cm. Again pulse duration $t_p = \pi/(2\gamma B_{\rm rf})$ s, $\mu_0 = 4\pi \times 10^{-7}$ Tm/A gives us $U_p \sim 9 \times 10^{-3}$ J.

As a result, we have $W < \Delta F < U_p$. Thus, our calculation of the cost of cooling the target qubit gives us a result larger than the work output of the quantum Otto engines and verifies the thermodynamical constraints.

[1] H. T. Quan, Yu-xi Liu, C. P. Sun, and F. Nori, Quantum thermodynamic cycles and quantum heat engines, Phys. Rev. E **76**, 031105 (2007).

[2] X.-L. Huang, X.-Y. Niu, X.-M. Xiu, and X.-X. Yi, Quantum stirling heat engine and refrigerator with single and coupled spin systems, Eur. Phys. J. D **68**, 32 (2014).

[3] G. Thomas and R. S. Johal, Friction due to inhomogeneous driving of coupled spins in a quantum heat engine, Eur. Phys. J. B **87**, 166 (2014).

[4] T. Zhang, W.-T. Liu, P.-X. Chen, and C.-Z. Li, Four-level entangled quantum heat engines, Phys. Rev. A **75**, 062102 (2007).

[5] X. L. Huang, H. Xu, X. Y. Niu, and Y. D. Fu, A special entangled quantum heat engine based on the two-qubit heisenberg *XX* model, Phys. Scr. **88**, 065008 (2013).

[6] G. Thomas and R. S. Johal, Coupled quantum otto cycle, Phys. Rev. E **83**, 031135 (2011).

[7] M. O. Scully, M. Suhail Zubairy, G. S. Agarwal, and H. Walther, Extracting work from a single heat bath via vanishing quantum coherence, Science **299**, 862 (2003).

[8] G. F. Zhang, Entangled quantum heat engines based on two two-spin systems with dzyaloshinski-moriya anisotropic antisymmetric interaction, Eur. Phys. J. D **49**, 123 (2008).

[9] S. Çakmak, F. Altintas, and Özgür E. Müstecaplıoğlu, Lipkin-meshkov-glick model in a quantum otto cycle, Eur. Phys. J. Plus **131**, 197 (2016).

[10] K. Zhang, F. Bariani, and P. Meystre, Quantum Optomechanical Heat Engine, Phys. Rev. Lett. **112**, 150602 (2014).

[11] D. Türkpençe and Özgür E. Müstecaplıoğlu, Quantum fuel with multilevel atomic coherence for ultrahigh specific work in a photonic Carnot engine, Phys. Rev. E **93**, 012145 (2016).

[12] S. Chand and A. Biswas, Single-ion quantum otto engine with always-on bath interaction, EPL Europhys. Lett. **118**, 60003 (2017).

[13] S. Chand and A. Biswas, Measurement-induced operation of two-ion quantum heat machines, Phys. Rev. E **95**, 032111 (2017).

[14] R. Uzdin, A. Levy, and R. Kosloff, Equivalence of Quantum Heat Machines, and Quantum-Thermodynamic Signatures, Phys. Rev. X **5**, 031044 (2015).

[15] A. Alecce, F. Galve, N. Lo Gullo, L. Dell'Anna, F. Plastina, and R. Zambrini, Quantum Otto cycle with inner friction: Finite-time and disorder effects, New J. Phys. **17**, 075007 (2015).

[16] H. E. D. Scovil and E. O. Schulz-DuBois, Three-Level Masers as Heat Engines, Phys. Rev. Lett. **2**, 262 (1959).

[17] R. Alicki, The quantum open system as a model of the heat engine, J. Phys. A: Math. Gen. **12**, L103 (1979).

[18] N. Linden, S. Popescu, and P. Skrzypczyk, How Small Can Thermal Machines Be? The Smallest Possible Refrigerator, Phys. Rev. Lett. **105**, 130401 (2010).

[19] R. Uzdin and R. Kosloff, The multilevel four-stroke swap engine and its environment, New J. Phys. **16**, 095003 (2014).

[20] D. Gelbwaser-Klimovsky, R. Alicki, and G. Kurizki, Minimal universal quantum heat machine, Phys. Rev. E **87**, 012140 (2013).

[21] R. Kosloff and A. Levy, Quantum heat engines and refrigerators: Continuous devices, Annu. Rev. Phys. Chem. **65**, 365 (2014).

[22] T. Feldmann and R. Kosloff, Quantum four-stroke heat engine: Thermodynamic observables in a model with intrinsic friction, Phys. Rev. E **68**, 016101 (2003).

[23] J. Roßnagel, S. T. Dawkins, K. N. Tolazzi, O. Abah, E. Lutz, F. Schmidt-Kaler, and K. Singer, A single-atom heat engine, Science **352**, 325 (2016).

[24] O. Abah, J. Roßnagel, G. Jacob, S. Deffner, F. Schmidt-Kaler, K. Singer, and E. Lutz, Single-Ion Heat Engine At Maximum Power, Phys. Rev. Lett. **109**, 203006 (2012).

[25] J. Klaers, S. Faelt, A. Imamoglu, and E. Togan, Squeezed Thermal Reservoirs As a Resource for a Nanomechanical Engine Beyond the Carnot Limit, Phys. Rev. X **7**, 031044 (2017).

[26] J. Roßnagel, O. Abah, F. Schmidt-Kaler, K. Singer, and E. Lutz, Nanoscale Heat Engine Beyond the Carnot Limit, Phys. Rev. Lett. **112**, 030602 (2014).

[27] R. Dillenschneider and E. Lutz, Energetics of quantum correlations, EPL (Europhys. Lett.) **88**, 50003 (2009).

[28] C. B. Dağ, W. Niedenzu, Özgür E. Müstecaplioğlu, and G. Kurizki, Multiatom quantum coherences in micromasers as fuel for thermal and nonthermal machines, Entropy **18**, 244 (2016).

[29] J. P. S. Peterson, T. B. Batalhão, M. Herrera, A. M. Souza, R. S. Sarthour, I. S. Oliveira, and R. M. Serra, Experimental characterization of a spin quantum heat engine, arXiv:1803.06021.

[30] R. J. de Assis, T. M. de Mendonça, C. J. Villas-Boas, A. M. de Souza, R. S. Sarthour, I. S. Oliveira, and N. G. de Almeida, Efficiency of a Quantum Otto Heat Engine Operating under a Reservoir at Effective Negative Temperatures, Phys. Rev. Lett. **122**, 240602 (2019).

[31] S. Çakmak, F. Altintas, A. Gençten, and Özgür E. Müstecaplıoğlu, Irreversible work and internal friction in a quantum otto cycle of a single arbitrary spin, Eur. Phys. J. D **71**, 75 (2017).

[32] D. K. Park, N. A. Rodriguez-Briones, G. Feng, R. Rahimi, J. Baugh, and R. Laflamme, Heat bath algorithmic cooling with spins: Review and prospects, in *Electron Spin Resonance (ESR) Based Quantum Computing*, edited by T. Takui, L. Berliner, and G. Hanson (Springer New York, New York, NY, 2016), pp. 227–255.

[33] N. A. Rodríguez-Briones and R. Laflamme, Achievable Polarization for Heat-Bath Algorithmic Cooling, Phys. Rev. Lett. **116**, 170501 (2016).

[34] Y. Atia, Y. Elias, T. Mor, and Y. Weinstein, Algorithmic cooling in liquid-state nuclear magnetic resonance, Phys. Rev. A **93**, 012325 (2016).

[35] G. Brassard, Y. Elias, J. M. Fernandez, H. Gilboa, J. A. Jones, T. Mor, Y. Weinstein, and L. Xiao, Experimental heat-bath cooling of spins, Eur. Phys. J. Plus **129**, 266 (2014).

[36] G. Brassard, Y. Elias, T. Mor, and Y. Weinstein, Prospects and limitations of algorithmic cooling, Eur. Phys. J. Plus **129**, 258 (2014).

[37] J. M. Fernandez, S. Lloyd, T. Mor, and V. Roychowdhury, Algorithmic cooling of spins: a practicable method for increasing polarization, Int. J. Quantum Inf. **02**, 461 (2004).

[38] Y. Elias, J. M. Fernandez, T. Mor, and Y. Weinstein, Optimal algorithmic cooling of spins, in *Unconventional Computation*, Lecture Notes in Computer Science, Vol. 4618, edited by S. G. Akl, C. S. Calude, M. J. Dinneen, G. Rozenberg, and H. T. Wareham (Springer, Berlin, Heidelberg, 2007), pp. 2–26.

[39] P. Oscar Boykin, T. Mor, V. Roychowdhury, F. Vatan, and R. Vrijen, Algorithmic cooling and scalable nmr quantum computers, Proc. Natl. Acad. Sci. **99**, 3388 (2002).

[40] D. Kafri and J. M. Taylor, Algorithmic Cooling of a Quantum Simulator, arXiv:1207.7111.

[41] S. Raeisi and M. Mosca, Asymptotic Bound for Heat-Bath Algorithmic Cooling, Phys. Rev. Lett. **114**, 100404 (2015).

[42] N. A. Rodríguez-Briones, J. Li, X. Peng, T. Mor, Y. Weinstein, and R. Laflamme, Heat-bath algorithmic cooling with correlated qubit-environment interactions, New J. Phys. **19**, 113047 (2017).

[43] C. A. Ryan, O. Moussa, J. Baugh, and R. Laflamme, Spin Based Heat Engine: Demonstration of Multiple Rounds of Algorithmic Cooling, Phys. Rev. Lett. **100**, 140501 (2008).

[44] L. J. Schulman, T. Mor, and Y. Weinstein, Physical Limits of Heat-Bath Algorithmic Cooling, Phys. Rev. Lett. **94**, 120501 (2005).

[45] Y. Elias, J. M. Fernandez, T. Mor, and Y. Weinstein, Optimal algorithmic cooling of spins, Isr. J. Chem. **46**, 371 (2006).

[46] I. S. Oliveira, T. J. Bonagamba, R. S. Sarthour, J. C. C. Freitas, and E. R. deAzevedo, 4-introduction to nmr quantum computing, in *NMR Quantum Information Processing* (Elsevier Science B.V., Amsterdam, 2007), pp. 137–181.

[47] M. Devoret, B. Huard, R. Schoelkopf, and L. F. Cugliandolo, *Quantum Machines: Measurement and Control of Engineered Quantum Systems: Lecture Notes of the Les Houches Summer School* (Oxford University Press, 2011).

[48] A. Abragam, Principles of nuclear magnetism, Am. J. Phys. **28**, 692 (1963).

[49] J. Goold, M. Huber, A. Riera, L. del Rio, and P. Skrzypczyk, The role of quantum information in thermodynamics'a topical review, J. Phys. A: Math. Theor. **49**, 143001 (2016).

[50] T. B. Batalhão, A. M. Souza, L. Mazzola, R. Auccaise, R. S. Sarthour, I. S. Oliveira, J. Goold, G. De Chiara, M. Paternostro, and R. M. Serra, Experimental Reconstruction of Work Distribution and Study of Fluctuation Relations in a Closed Quantum System, Phys. Rev. Lett. **113**, 140601 (2014).

[51] S. Lloyd, Quantum-mechanical maxwell's demon, Phys. Rev. A **56**, 3374 (1997).

[52] S. Y. Hou, Y. B. Sheng, G. R. Feng, and G. L. Long, Experimental optimal single qubit purification in an NMR quantum information processor, Sci. Rep. **4** (2014).

[53] Z. Li, M. H. Yung, H. Chen, D. Lu, J. D. Whitfield, X. Peng, A. Aspuru-Guzik, and J. Du, Solving quantum ground-state problems with nuclear magnetic resonance, Sci. Rep. **1** (2011).

[54] M. K. Henry, J. Emerson, R. Martinez, and D. G. Cory, Localization in the quantum sawtooth map emulated on a quantum-information processor, Phys. Rev. A **74**, 062317 (2006).

[55] H. K. Cummins, C. Jones, A. Furze, N. F. Soffe, M. Mosca, J. M. Peach, and J. A. Jones, Approximate Quantum Cloning with Nuclear Magnetic Resonance, Phys. Rev. Lett. **88**, 187901 (2002).

[56] R. Kosloff, Quantum thermodynamics: A dynamical viewpoint, Entropy **15**, 2100 (2013).

[57] S. Vinjanampathy and J. Anders, Quantum thermodynamics, Contemp. Phys. **57**, 545 (2016).

[58] B. Gardas and S. Deffner, Thermodynamic universality of quantum Carnot engines, Phys. Rev. E **92**, 042126 (2015).

[59] A. Ü. C. Hardal and Özgür E. Müstecaplıoğlu, Superradiant quantum heat engine, Sci. Rep. **5**, 12953 (2015).

[60] A. G. Redfield, On the theory of relaxation processes, IBM J. Res. Dev. **1**, 19 (1957).

[61] F. Clivaz, R. Silva, G. Haack, J. B. Brask, N. Brunner, and M. Huber, Unifying paradigms of quantum refrigeration: A universal and attainable bound on cooling, arXiv:1903.04970v1.

[62] F. Clivaz, R. Silva, G. Haack, J. B. Brask, N. Brunner, and M. Huber, Unifying paradigms of quantum refrigeration: fundamental limits of cooling and associated work costs, arXiv:1710.11624v3.

[63] M. Esposito and C. Van den Broeck, Second law and landauer principle far from equilibrium, EPL (Europhys. Lett.) **95**, 40004 (2011).